Available online at www.sciencedirect.com

ScienceDirect

Procedia Engineering 168 (2016) 646 – 649

Procedia Engineering

www.elsevier.com/locate/procedia

30th Eurosensors Conference, EUROSENSORS 2016

LTCC and thick-film ceramic magnetic sensors for tokamak nuclear fusion

Thomas Maeder[a]*, Caroline Jacq[a], Duccio Testa[b], Matthieu Toussaint[b], Martin Stöck[ab], Adrien Corne[ab], Lucas Güniat[ab], Benoît Ellenrieder[ab], Xinyue Jiang[a], Philipp Windischhofer[ab], Christian Schlatter[b], Peter Ryser[a]

[a]*Laboratoire de Production Microtechnique, EPFL, CH-1015 Lausanne, Switzerland*
[b]*Swiss Plasma Center, EPFL, CH-1015 Lausanne, Switzerland*

Abstract

The present contribution gives an overview of our work on non-conventional magnetic coil sensors for diagnostics and plasma stability control of nuclear fusion experiments in tokamaks. Instead of wire wound around a core, these devices consist of printed conductor wire coils on ceramic substrates, and are based on LTCC (low-temperature co-fired ceramic) and thick-film technology, which allow creation of monolithic multilayer coils with excellent stability. For 3D sensing, an innovative modular design combining LTCC coils and an alumina base has been developed. Finally, the important aspects of integration, manufacturing, mounting and interconnection are discussed.
© 2016 The Authors. Published by Elsevier Ltd. This is an open access article under the CC BY-NC-ND license (http://creativecommons.org/licenses/by-nc-nd/4.0/).
Peer-review under responsibility of the organizing committee of the 30th Eurosensors Conference

Keywords: nuclear fusion ; tokamak ; magnetic confinement ; magnetic sensors ; ceramics ; LTCC ; thick-film technology

1. Introduction & ceramic technologies for magnetic coils

Nuclear fusion experiments using magnetic confinement in tokamaks require extensive monitoring of the magnetic field distribution, in order to detect and counteract instabilities in the plasma over a wide range of frequencies [1]. In an actual fusion generating plant, corresponding sensors must endure extreme environments, mainly high temperature (up to ~300°C) and intense, high-energy neutron bombardment. Classically, magnetic

* Corresponding author. Tel.: +41 21 693 58 23; fax: +41 21 693 38 91.
E-mail address: thomas.maeder@alumni.epfl.ch

1877-7058 © 2016 The Authors. Published by Elsevier Ltd. This is an open access article under the CC BY-NC-ND license (http://creativecommons.org/licenses/by-nc-nd/4.0/).
Peer-review under responsibility of the organizing committee of the 30th Eurosensors Conference
doi:10.1016/j.proeng.2016.11.235

fields in tokamaks are sensed using Mirnov-type coils, consisting of a metallic wire wound around a ceramic core [2]. This design, however, is bulky and unpractical for multidimensional 3D sensing of the normal (Z), toroidal (X) and poloidal (Y) magnetic fields, and the thin wire poses reliability issues due to e.g. parasitic plasmas and differential thermal expansion. Therefore, monolithic ceramic sensor coils based on LTCC have been investigated [2–4], where the coil wiring is embedded inside ceramic layers. Similar monolithic sensors have been proposed for 3D sensing [5], but face drastic yield issues given the very high number of required vias to form the vertical part of the X and Y coils. We therefore have introduced an innovative modular concept [2,6] (Fig. 1de, Fig. 3abc), with an alumina ceramic substrate comprising a thick-film printed Z coil and carrying a series of simple, identical edge-mounted LTCC modular coils for X and Y sensing. The present contribution gives an overview of our work on these sensors, and discusses their design and optimisation, as well as the important aspects of integration, manufacturing, mounting and interconnection.

Besides classical thick-film technology [7], where layers are printed and fired successively onto a pre-fired substrate, typically alumina, there are two common inherently multilayer ceramic technologies, LTCC [8] and HTCC [9], (low, high-temperature co-fired ceramic), where conductors are printed onto unfired dielectric tapes, with the whole stack being laminated and co-fired at the end. Typical technological characteristics are given in Table 1, and lead us to believe that LTCC is the most favourable technology for coils, as Ag, Au and Cu feature low resistivity, and the equipment / processing requirements are modest compared to HTCC. Classical thick-film technology features very similar materials, but the requirement of printing the dielectric limits its practical thickness and thereby increases both inductive and capacitive coupling between each winding layer. Nevertheless, technological intermediates are also possible, such as LTTT (low-temperature transfer tape), a variant of LTCC allowing sequential lamination and firing of thicker dielectric onto alumina substrates [10].

Table 1. Typical characteristics of thick-film based multilayer technologies [7–10].

Technology	Classical thick-film	LTCC	HTCC
Substrate	Alumina (pre-fired)	Glass-ceramic tape (co-fired)	Alumina (co-fired)
Insulating dielectric	Glass-ceramic (printed ink)	*Same as substrate*	*Same as substrate*
Conductors (base)	Ag, Au, Cu, Pt	Ag, Au, Cu, Pt	Mo, W, Pt
Firing temperature	850°C	850-900°C	1400°C
Firing atmosphere	Air (Cu:N_2)	Air (Cu:N_2)	N_2:H_2:H_2O
Advantages	Straightforward, reliable processing (layer-by-layer checking possible), moderate firing conditions & good dimensional control	Simple build-up of layers Moderate firing conditions	Simple build-up of layers
Issues	Slow; many firing steps Difficult to build up dielectric thickness (but can use LTTT instead of printing dielectric)	Control of lamination and shrinkage (interaction of dielectric tape and conductors); layer-by-layer checking impossible – tight process control required HTCC: higher infrastructure requirements or use very expensive Pt; higher resistivity of conductors	

2. Magnetic coil design

A monolithic LTCC coil basically has the structure shown in Fig. 1a, i.e. consists in a stack of LTCC layers, printed with conductor ink spiralling alternatively inwards and outwards. Fig. 1ab also shows different possible parameters, whose selection has to integrate the following, partly conflicting requirements: high signal, i.e. NA_{eff}, high resonance frequency f_{res}, compact size and moderate complexity, i.e. moderate cost and good production yield.

- **Effective area**. From Fig. 1a, it can be seen that for a specific size, a given NA_{eff} value may be obtained by several combination of turns per layer MM and number of active layers NN, for a total number of turns $N = NN \times MM$. Modelling each winding layer as a series of concentric rounded rectangles with outer winding ($k = 1$) dimensions $a \times b$, a constant corner radius R and inter-track pitch p, the effective area for each winding k can be estimated according to eq. (1). This is shown for the data of the 1D HF sensor [3] in Fig. 2a, with good agreement between this calculation and the measured values for many sensors with $MM = 5$, 10 and 20. While

increasing *MM* carries little additional complexity (change of printing mask only) and is therefore preferred in terms of cost and production yield, the last inner turns contribute little to NA_{eff}. On the other hand, increasing *NN* yields a linear increase in NA_{eff}, which is shown in Fig. 2b for the data of ref. [3], albeit at the cost of more manufacturing complexity.

$$NA_{\text{eff},k} = [a-(k-1)\cdot p]\cdot[b-(k-1)\cdot p]-(4-\pi)\cdot R^2 \tag{1}$$

- **Resonance frequency**. Assuming a simple one-pole model, the resonance frequency f_{res} can be estimated according to eq. (2). Considering the sensor (C_{self}, L_{self}) and cable (C_{cable}, L_{cable}) characteristics (Table 2 [3]) for a sensor with NA_{eff} ~ 0.05 m^2, the required value, one sees that C is dominated by the cable, and L by the sensor, which implies the main goal to maximise f_{res} is to decrease L_{self} for a given NA_{eff}. This is in principle possible by making the sensor thicker (increasing *NN*), for a given set of outer coil dimensions (*a*, *b*, *R*), but yields in practice limited improvements unless the total thickness between top and bottom coils, *h* is increased drastically, as e.g. attested by well-known short-coil approximations [11] and the results in ref. [3], which show a difference of only ~10% in the corresponding figure of merit, $u = NA_{eff} / L_{self}^{0.5}$ ~ 21-23 cm^2/μH$^{0.5}$ between the worst and best samples (Fig. 2c). Increasing the coil in-plane dimensions, if possible, is favourable, as L scales very roughly with $N^2 \cdot a$ (if $b \sim a$), whereas NA_{eff} does so with $N \cdot a^2$, i.e. u and f_{res} approximately scales with $a^{1.5}$. This is illustrated by the values of u ~ 10 and 65 cm^2/μH$^{0.5}$ for the small LTCC modules of the 3D sensor (Fig. 1d) and the large Z coil (Fig. 1e) respectively [6].

$$f_{\text{res}}^{-1} = 2\pi\sqrt{L\cdot C} \sim 2\pi\sqrt{L_{\text{self}}\cdot C_{\text{cable}}}\text{, where } L \approx L_{self} + L_{cable} \text{ and } C \approx C_{self} + C_{cable} \tag{2}$$

- **3D sensor, X & Y sensing**. For the 3D sensor [6] (Fig. 1de & 3abc), both NA_{eff} and u of the LTCC modular coils, limited by space requirements, are improved by "numbering up", i.e. placing 10 coils in series for each direction (Fig. 2de & 3a). Mutual coupling is limited, yielding only a moderate increase (~30%) of L_{self} vs 10 isolated coils. This solution is both economical and reliable (high-yield manufacturing of many simple, small coils that can be tested before mounting), provided the assembly technique is robust.

Table 2. Typical sensor / cable inductances & capacitances.

Item	Cable	1D sensor ("20t8c" [3])	Sensor:cable ratio
Capacitance *C*	C_{cable} ~ 500 pF (~50 m, ~10 pF/m) [3]	C_{self} = 33 pF	~1:15
Inductance *L*	L_{cable} ~ 15 μH (~50 m, ~0.3 μH/m) [3]	L_{self} = 519 μH	~35:1

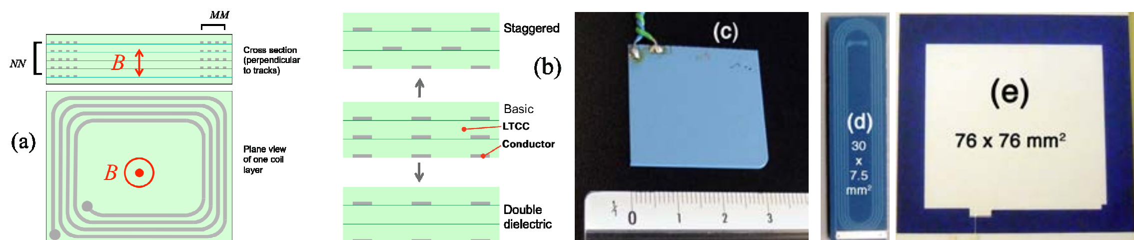

Fig. 1. Schematic ceramic coil build-up – a) basic coil consisting of a stack of LTCC tapes printed with the winding conductor; winding parameters *MM* = number of turns per layer and *NN* = number of layers; b) stacking parameters – basic (turns simply superposed), staggered to reduce capacitance or with thicker dielectric obtained by inserting an additional LTCC tape between each winding layer; c) 1D HF sensor [3]; d) 3D HF sensor LTCC coil module for X-Y sensing [6], and e) bottom of substrate of same 3D sensor, with Z coil beneath blue dielectric.

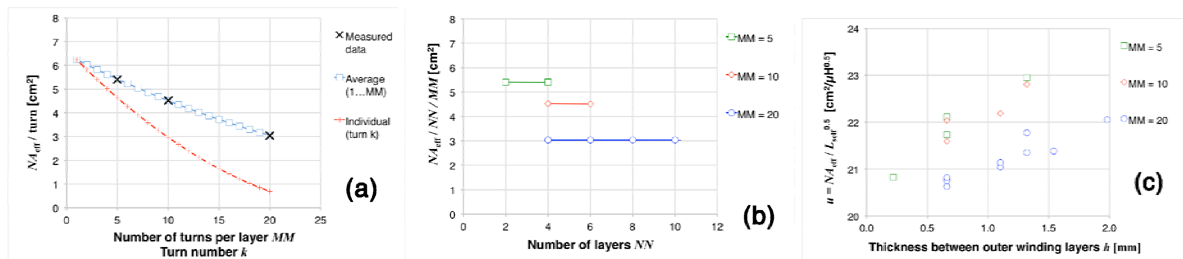

Fig. 2. 1D HF coil [3]: ab) signal per turn in layer vs *MM* and *NN*; c) signal-inductance figure of merit vs overall winding thickness.

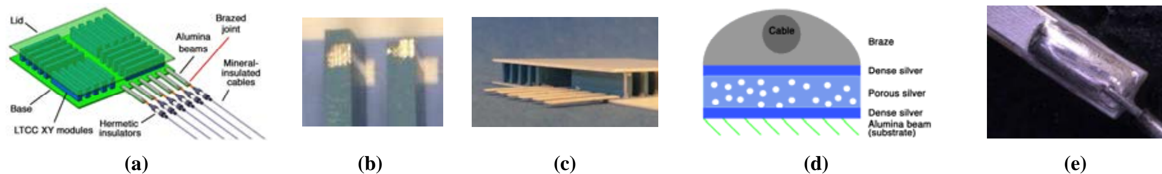

Fig. 3. Packaging: overall 3D sensor construction and connection [6] (a); fritted Ag ink for edge bonding LTCC XY coils to base (bc), to lid (c) as well as for bonding alumina beams to base (c); porous Ag used to decouple thermal stresses between braze and alumina beam (de).

3. Conclusions and outlook – assembly, packaging and interconnection

Whereas high-frequency (HF) 1D [3] and 3D [6] ceramic sensors have been demonstrated, the solutions applied for assembly, packaging and interconnection, illustrated in Fig. 3 [6,12,13], are less mature. The overall concept for the 3D sensor is shown in Fig. 3a. The LTCC coils are bonded to the base and lid (Fig. 3abc) using a glass-fritted Ag conductor, which also provides for coil-base electrical connections; the same technique is used for the small metallised alumina beams that allow brazing of the cables (Fig. 3ac). As the strong thermal mismatch between braze and ceramic can cause cracking of the latter, a porous metallisation has been formulated (Fig. 3d) to decouple the stress, allowing reliable brazed bonds [12]. Overall, this solution remains cumbersome, as the sensor and cables must be linked prior to installation inside the tokamak. Therefore, work has been initiated to replace the alumina beams with wire segments [13], which potentially allow much more convenient separate installation of MI cabling and sensor, the final link being made by e.g. crimping or with a screw terminal.

References

[1] D. Testa, H. Carfantan, M. Toussaint, R. Chavan, Y. Fournier, J. Guterl, J.B. Lister, T. Maeder, J.M. Moret, A. Perez, F. Sanchez, B. Schaller, C. Slater, M. Stoeck, G. Tonetti, Fusion Eng. Des. 86 (2011) 1149–1152.
[2] M. Toussaint, D. Testa, N. Baluc, R. Chavan, Y. Fournier, J.B. Lister, T. Maeder, P. Marmillod, F. Sanchez, M. Stöck, Fusion Eng. Des. 86 (2011) 1248–1251.
[3] D. Testa, Y. Fournier, T. Maeder, M. Toussaint, R. Chavan, J. Guterl, J.B. Lister, J.M. Moret, B. Schaller, G. Tonetti, Fusion Sci. Technol. 59 (2011) 376–396.
[4] S. Peruzzo, S. Arshad, M. Brombin, G. Chitarin, W. Gonzalez, L. Grando, M. Portales, A. Rizzolo, G. Vayakis, Fusion Eng. Des. 88 (2013) 1302–1305.
[5] H. Takahashi, S. Sakakibara, Y. Kubota, H. Yamada, Rev. Sci. Instrum. 72 (2001) 3249–3259.
[6] D. Testa, A. Corne, G. Farine, C. Jacq, T. Maeder, M. Toussaint, Fusion Eng. Des. 96-97 (2015) 989–992.
[7] W. Borland, in:, Electron. Mater. Handb. Vol 1 Packag. ASM, 1989, pp. 332–353.
[8] C.J. Sabo, W.A. Vitriol, C.L. Slaton, D.L. Rychlick, in:, Ceram. Substrates Packag. Electron. Appl. Adv. Ceram. Vol 26, 1989, pp. 217–228.
[9] R.R. Tummala, Am. Ceram. Soc. Bull. 67 (1988) 752–758.
[10] R.K. Yamamoto, M.R. Gongora-Rubio, R.S. Pessoa, M.R. da Cunha, H.S. Maciel, J. Microelectron. Electron. Packag. 6 (2009) 101–107.
[11] H.A. Wheeler, Proc. Inst. Radio Eng. 16 (1928) 1398–1400.
[12] C. Jacq, T. Maeder, L. Güniat, A. Corne, D. Testa, P. Ryser, in:, Proc. IMAPSACerS 11th Int. CICMT Conf., Dresden (DE), 2015, pp. 234–238.
[13] C. Jacq, T. Maeder, M. Toussaint, B.R. Ellenrieder, P. Windischhofer, X. Jiang, D. Testa, P. Ryser, in:, Proc. 12th IMAPSACerS Int. Conf. Ceram. Interconnect Ceram. Microsyst. Technol. CICMT, Denver (USA), 2016, pp. 58–63.